Histologic models for optical tomography and spectroscopy of tissues

Rohit Bhargava* and Brynmor J. Davis
Department of Bioengineering and the Beckman Institute for Advanced Science and Technology,
University of Illinois at Urbana-Champaign, 405 North Mathews Ave., Urbana, IL USA 61801

ABSTRACT

Histologic information is often the ground truth against which imaging technology performance is measured. Typically, this information is limited, however, due to the need to excise tissue, stain it and have the tissue section manually reviewed. As a consequence, histologic models of actual tissues are difficult to acquire and are generally prohibitively expensive. Models and phantoms for imaging development, hence, have to be simple and reproducible for concordance between different groups developing the same imaging methods but may not reflect tissue structure. Here, we propose a route to histologic information that does not involve the use of human review nor does it require specialized dyes or stains. We combine mid-infrared Fourier transform infrared (FT-IR) spectroscopy with imaging to record data from tissue sections. Attendant numerical algorithms are used to convert the data to histologic information. Additionally, the biochemical nature of the recorded information can be used to generate contrast for other modalities. We propose that this histologic model and spectroscopic generation of contrast can serve as standard for testing and design aid for tomography and spectroscopy of tissues. We discuss here the biochemical and statistical issues involved in creating histologic models and demonstrate the use of the approach in generating optical coherence tomography (OCT) images of prostate tissue samples.

Keywords: Spectroscopy, histology, Fourier transform infrared spectroscopic imaging, FT-IR, optical coherence tomography, modeling, microscopy, simulation, software phantom, prostate

1. INTRODUCTION

Histopathology is the gold standard for evaluation of microscopic imaging technologies. In particular, correlative information for the evaluation of *in-vivo* imaging technologies usually consists of a corresponding hematoxylin and eosin (H&E) stained image of the excised tissue. Most often, data from an imaging technology are presented side-by-side with the corresponding H&E image. In general, the confirmatory correlation sought is a visual cue that replicates the contrast of H&E images by the particular contrast of the imaging modality. In some cases, contrast information from multiple imaging modalities and dyes can be combined in efforts to reproduce the observed H&E structure. There are few reports, however, on using histopathology as a basis for the development of imaging technologies. In particular, the use of histologic ground truth can help simulate the forward problem and help understand a modality's performance under different experimental parameters, quality of data obtained and potential distortions that may be encountered. Unfortunately, histologic ground truth is not readily available for such use due to the need to stain tissue and the manual nature of examinations.

A new concept has recently emerged in which chemical imaging can be used to measure the intrinsic biochemical content of tissue and employ the same for histologic recognition. The method does not require dyes but relies on spectral data recording. Instead of relying on a human (pathologist) to make decisions, objective numerical algorithms are employed to segment tissue. In one such effort, infrared spectroscopy is used in an imaging format to measure the content of tissue. While efforts to describe tissue using IR spectroscopy are nearly 60 years old, advances in both instrumentation and computational capability have revolutionized this area of investigation [1]. Studies are now being published that involve statistically significant populations of patients (>100), millions of spectral measurements and detailed understanding due to new computational algorithms. The instrumentation advances have mostly centered around the development of Fourier transform infrared (FT-IR) spectroscopic imaging [1, 2, 3].

* rxb@illinois.edu; http://cisl.bioen.illinois.edu

Optical Tomography and Spectroscopy of Tissue VIII, edited by Bruce J. Tromberg, Arjun G. Yodh, Mamoru Tamura, Eva M. Sevick-Muraca, Robert R. Alfano, Proc. of SPIE Vol. 7174
71742H · © 2009 SPIE · CCC code: 1605-7422/09/$18 · doi: 10.1117/12.810119

FT-IR imaging combines the imaging capabilities of optical microscopy with the chemical selectivity of FT-IR spectroscopy. Similar to optical microscopy, FTIR imaging of tissue provides images. At each pixel, additionally, is a spectrum that depends uniquely on the sample's chemical composition. IR absorption spectra are, thus, a unique and quantitative "fingerprint" of composition. FTIR spectroscopy is well established for the high-throughput, non-invasive and non-destructive recording of molecular vibrational modes [4]. While not as molecularly specific as some techniques (e.g. mass spectroscopy), spectra provide holistic measurements rapidly and reproducibly [5]. Correspondingly, contrast in FTIR images [6] is generated using algorithms to find differences in tissue chemistry. For example, by selecting appropriate spectral parameters, one is able to "dial" a specific chemistry. Instead of recognizing microscopic structural patterns, we have recently demonstrated an alternate approach to prostate histopathology by directly measuring tissue chemistry [7]. Since both tissue structure and chemical composition are measured, the process is also termed chemical imaging.

A number of laboratory studies have demonstrated carefully biochemical changes indicative of disease [8], determined optical [9] and biological confounding factors [10,11] and demonstrated preliminary potential [12]. Until recently, there was a general lack of substantially validated protocols to perform automated tissue recognition with FT-IR imaging. The primary reason was the slow nature of data acquisition and the trade-off between light intensity and spatial resolution in FT-IR microscopy that prevented validations on large (hundreds) of samples. The drawbacks have been addressed by new technologies and high-throughput sampling methods. For example, a recent report combined FT-IR imaging with combinatorial tissue microarrays (TMA), fast numerical processing and statistical tests [13]. The study developed both objective protocols as well as performed substantial validation [14]. Following the study, protocols to classify tissue into one of ten cell types without human input and without using any stains are available. The net result is that color-coded images of tissue are available that correspond to each cell type. The large population sampling provides an estimate of statistical variance that captures heterogeneity in measurements. The TMA results can be translated to larger, radical prostatectomy (RP) samples or whole mounts without any protocol modifications but few studies have actually demonstrated that result.

In this manuscript, we propose to utilize the advances in automated histologic classification to provide an image that can be used to predict the response of another optical imaging modality. The modality chosen as a demonstrative example is optical coherence tomography (OCT) [15,16,17]. In OCT reflections of low-coherence light are detected permitting the imaging of tissue microstructure in-situ. Micron-scale resolution images can be obtained without the need for excision and histological processing, and the technology has been applied for imaging a wide range of nontransparent tissues [18,19,20,21,22,23]. Imaging depths of 1-2 mm, resolutions of less than 2 μm [24,25] and real-time image acquisition have all been demonstrated [26] using probes [27,28] and for both animal models and humans [29]. The information content of OCT, however, is limited to linear scattering (structure) visualization and will require an expert to interpret data and make decisions. While efforts have been made towards extending OCT for molecular imaging of biological tissue [30,31,32] the gold standard for comparison has generally been H&E images. To simulate the forward problem, the usual approach is to model and validate on spheres suspended in a liquid [33]. Here we show that IR imaging results can be employed to generate computationally the likely image that would be obtained by OCT. A limited set of physical effects is modeled in this preliminary communication but the major idea of using validated histology to simulate image formation in an optical imaging modality is proposed and broadly demonstrated.

2. EXPERIMENTAL

Spectroscopic imaging data sets were acquired for small sample regions separately by averaging two interferometer scans at 4cm^{-1} spectral resolution, and a moving mirror speed of 2.2cm/s on the Perkin-Elmer Spotlight 400 imaging spectrometer with a linear array detector and a raster scanning technique. A NB-medium apodization and undersampling ratio of 2 (referenced to a He-Ne laser) are employed in data collection. As the peaks of interest are the fundamental vibrational modes and the substrate cutoff is approached around 700 cm^{-1}, the free-scanning spectral range is truncated to 4000-720 cm^{-1} for optimal information content and storage. Each pixel in the image recorded was corresponds 6.25μm square at the sample. An IR background is collected with 120 scans per pixel at a location on the substrate with no tissue present and the ratio of the background to sample intensity is computed. Any remaining vapor artifacts are removed from the spectral data using the Perkin-Elmer Spotlight atmospheric correction algorithm. A formalin-fixed, paraffin-embedded radical prostatectomy sample was obtained from an anonymized donor in the NIH tissue array research program. A thin (~5 μm) section of the tissue was microtomed and placed onto a BaF_2 disk. The sample was washed in

hexane for 24 hours and paraffin was removed. Data were processed following previously described procedures [34]. Figure 1 shows the class image obtained after automated tissue segmentation. Figure 2 shows the distribution of protein in tissue based on the Amide I vibrational mode, which is roughly indicative of density differences between tissues.

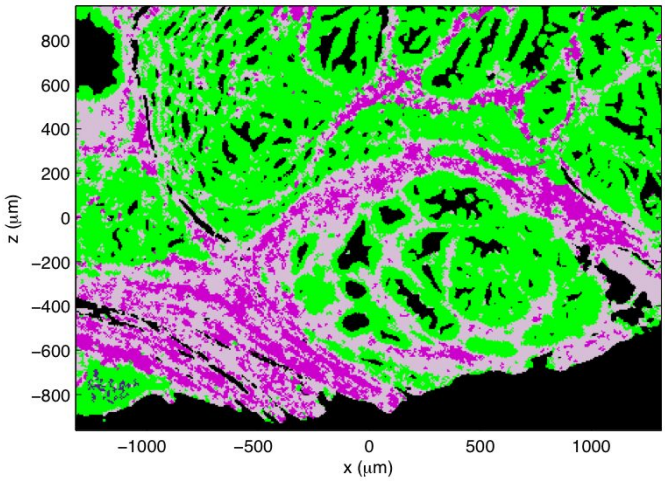

Fig. 1. Classified image of a section of prostate tissue in which colors denote specific cell types. Epithelium, fibroblast-rich stroma and largely extra-cellular matrix classes are denoted by green, magenta and thistle colors respectively.

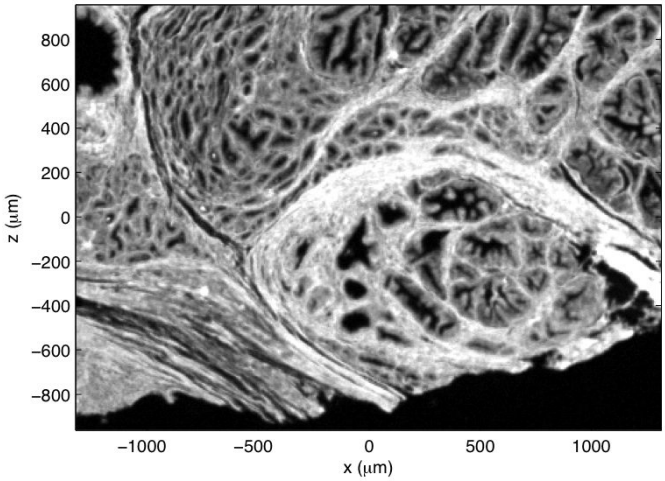

Fig. 2. Grayscale image demonstrating the relative distribution of the Amide I vibrational mode absorbance within tissue. The texture in the image is roughly indicative of the density changes in the structure of the tissue.

3. MODELING

3.1 Transformations between tissue properties

While different imaging techniques operate using different contrast mechanisms, e.g., scattering, absorption, fluorescence, etc., it is generally assumed that contrast is directly correlated to object structure. Consequently, one can reasonably produce mappings between tissue properties using relatively simple, local, mathematical operations. For example, each of the tissue types in Fig. 1 can be modeled as having a different refractive index in the near infrared. Defining an arbitrary unit of index contrast Δn, and assigning refractive indices $(1+\Delta n)$ to epithelium, $(1+1.6\Delta n)$ to

extra-cellular matrix, and $(1+2.4\Delta n)$ to fibroblast-rich stroma, results in the index map seen in Fig. 3. Alternatively, one can directly associate the grayscale values in Fig. 2 with the refractive index contrast.

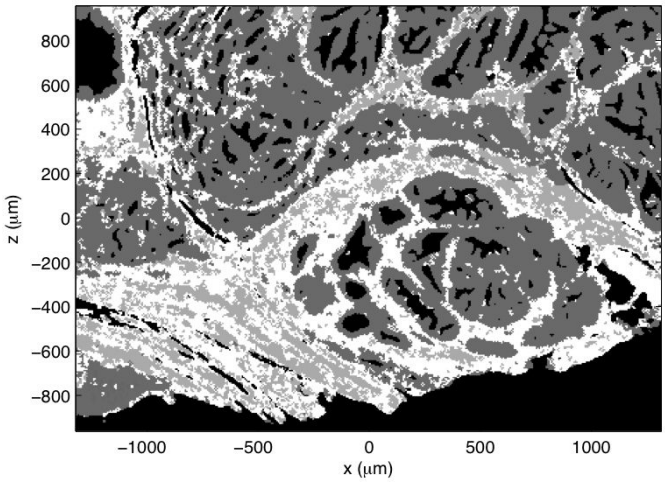

Fig. 3. A near-infrared index contrast or scattering potential (Δn) image calculated by assigning a different refractive index to each class in Fig. 1.

3.2 Simple simulation of OCT image formation

Starting with the maps of scattering potential based on Fig. 2 or as shown in Fig. 3, it is possible to simulate OCT imaging. OCT is a coherent imaging technique that uses low-coherence interferometry to resolve sample structure in the axial (depth) direction and scanning of the focus to resolve transverse structure. Modern OCT systems often collect data in the spectral domain, as spectroscopic data collection offers significant advantages in terms of speed and signal strength [35,36]. Mathematically, two-dimensional spectral OCT data, *S*, can be expressed [37] as

$$S(x,k) = A(k)\int g^2(x,z,k)\Delta n(x,z)dz \ , \qquad (1)$$

where k is wavenumber (the spectral axis), A is a factor dependent on the spectral profile of the optical source and g is the focused field produced by the objective lens. It should be noted that this model employs the first Born approximation, i.e., only singly scattered light is considered. Multiply scattered light does not contribute to the usable image in OCT and results in image artifacts.

In the simple model used here, the illumination source is assumed to have a flat emission profile over the collected bandpass and a Gaussian beam [38] describes the focused field. An objective numerical aperture of 0.025 is simulated and the spectrometer is modeled as collecting 160 data points over a spectral range corresponding to wavelengths between 980nm and 1020nm. With these parameters the transverse resolution of the system is approximately 25.5μm (calculated from the Gaussian beam waist) and the depth of focus is approximately 1020μm (calculated from the Rayleigh range).

To a first approximation, the relation described in Eq. (1) can be inverted by taking an inverse Fourier transform over the k axis. The axial resolution of the system is defined by the bandwidth of the source and for the parameters simulated here, this gives a value of approximately 12.5μm. Equation (1) was evaluated for the scattering potentials shown in both Fig. 2 and Fig. 3, and OCT images calculated – the image from Fig. 2 is shown in Fig. 4, and the image from Fig. 3 is shown in Fig. 5. The difference between the images illustrates the basis of contrast. If simple density changes are considered, Fig. 4 provides an image in which the contrast between the classes is limited (cf. Fig. 1). In the case where properties of cell types are explicitly considered, the contrast between classes is accurately reflected in the image.

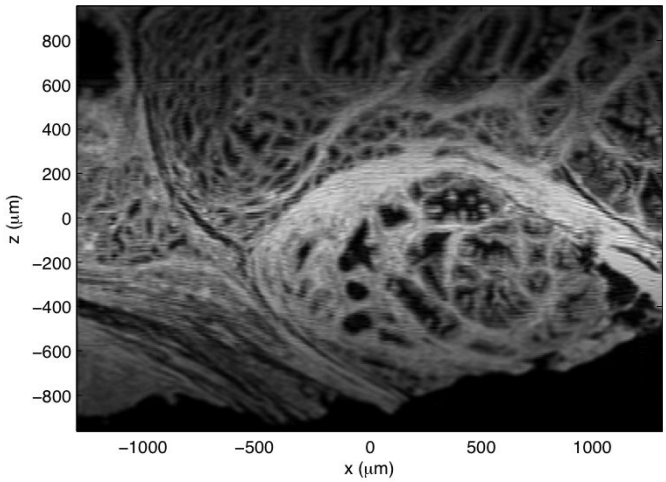

Fig. 4. A simulated OCT image calculated from the scattering potential of Fig. 2. The axial dimension is in z and the transverse dimension is x. The focus of the objective lens is at the z=0 plane and the probing light is assumed to be incident from the bottom of the image.

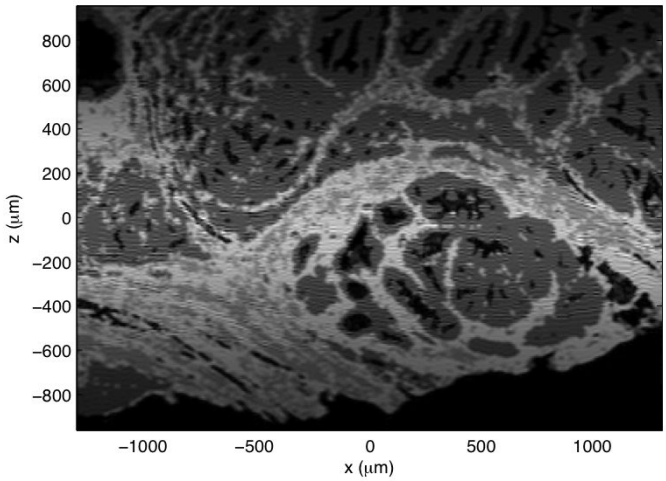

Fig. 5. A simulated OCT image calculated from the scattering potential of Fig. 3.

The effects of the limited OCT resolution can be seen in both images. Also visible is the loss signal strength as one moves outside of the depth of focus. Standard OCT image reconstruction breaks down outside of the depth of focus, resulting in transverse blurring and a rapid decay in signal strength. However, more advanced image reconstruction techniques can be applied to eliminate the transverse blurring and lessen the signal decay [33,39] – these methods could be applied to the simulated data but are not considered here.

3.3 Including noise and absorption

Absorption and multiple scattering limit the depth of imaging achievable in OCT. These effects are not captured in the linearized model of Eq. (1), as applying the first Born approximation involves assuming that the illuminating field at a point is not appreciably affected by the rest of the sample. An exact accounting of absorption and multiple scattering can be difficult, since both effects are non-local, i.e., the absorption of the field to a given point depends on the entire propagation path of the incident light, and the strength of the multiply scattered field at a point depends on the scattering from all neighboring points. However, as a first approximation, the sample absorption can be modeled with a homogeneous absorption coefficient. For a well-collimated beam the incident field will then decay exponentially into the sample. The incident field in Eq. (1) is then replaced by

$$g(x,z,k) \to g(x,z,k)\exp(-\alpha k z), \tag{2}$$

where α is the absorption coefficient. This modified forward model was applied to the index map seen in Fig. 3 and the corresponding OCT images are displayed in Fig. 6. Three different absorption coefficients were simulated and it can be seen that the absorption does indeed limit the depth of imaging in these simulations.

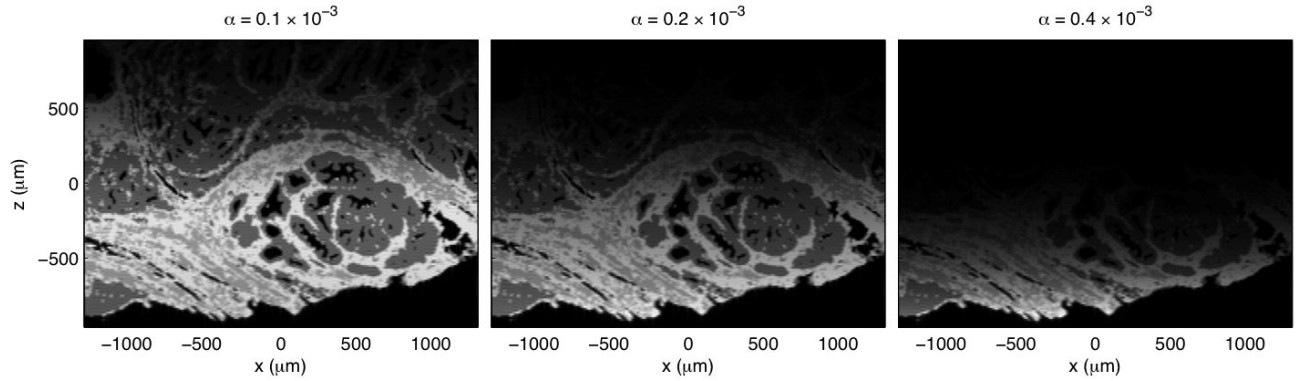

Fig. 6. Simulated OCT images calculated with a forward model that includes absorption. Three different absorption coefficients are simulated, resulting in three differing penetration depths for the illuminating light.

Noise can also be a crucial limiting factor in the performance of OCT imaging systems. Fluctuations of the interferometer reference beam often dominate the statistics, and so noise can be reasonably modeled as Gaussian and spatially independent in the image domain (see Ref. 36 for a more detailed OCT noise model). The effects of noise on the image are illustrated in Fig. 7. In this figure the signal to noise ratio (SNR) is defined as $20\log_{10}(P/\sigma)$, where P is the peak value of the image and σ is the standard deviation of the Gaussian noise.

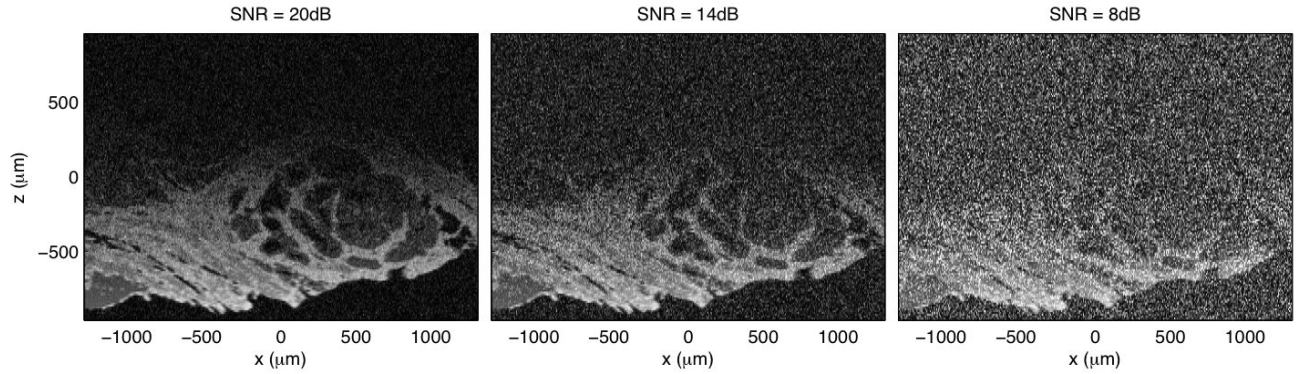

Fig. 7. The $\alpha=0.2\times10^{-3}$ image of Fig. 6 corrupted by varying amounts of measurement noise. All of these images are displayed on the same scale with some high-noise, high-signal pixels saturating the color map.

4. CONCLUSIONS

The use of histologic models derived from spectroscopic imaging and automated analysis of clinical samples has been proposed in this manuscript. While the technology to extract histologic ground truth is becoming readily available and used by many practitioners, the use of such information to model and understand other imaging systems has not been demonstrated. A simple set of image formation steps and effects of experimental parameters were implemented in this manuscript to simulate OCT images from the corresponding class images and spectral texture. The effects of using both approaches, idealized sample absorption and noise can be seen in the generated images. It is anticipated that the methodology proposed here will be refined and may prove useful in the modeling, design and evaluation of imaging instruments for specific tissue types.

ACKNOWLEDGEMENTS

This study was supported in part by a DoD Young Investigator Award in the prostate cancer research program and a grant from the Grainger Foundation. We gratefully acknowledge the prostate tissue samples and many discussions with Dr. Stephen M. Hewitt, National Cancer Institute.

REFERENCES

[1] The state of the art in this field is summarized in a recent volume, Bhargava, R. and Levin, I. W., eds., [Spectrochemical Analysis Using Infrared Multichannel Detectors], Blackwell Publishing, Oxford, (2005).

[2] Lewis, E. N., Treado, P. J., Reeder, R. C., Story, G. M., Dowrey, A. E., Marcott, C. and Levin, I. W., "Fourier transform spectroscopic imaging using an infrared focal-plane array detector," Anal. Chem. 67, 3377-3384 (1995).

[3] Bhargava, R. and Levin, I. W., "Fourier transform infrared imaging: theory and practice," Anal. Chem. 73, 5157-5167 (2001).

[4] Diem, M., Romeo, M., Boydston-White, S., Miljkovic, M. and Matthaus, C., "A decade of vibrational micro-spectroscopy of human cells and tissue (1994-2004)," Analyst 129, 880-885 (2004).

[5] Many issues are summarized in Jackson, M., "From biomolecules to biodiagnostics: spectroscopy does it all," Faraday Discuss. 126, 1-18 (2004).

[6] Koenig, J. L., Wang, S. Q. and Bhargava, R., "FTIR images," Anal. Chem. 73, 360A-369A (2001).

[7] Fernandez, D. C., Bhargava, R., Hewitt, S. M. and Levin, I. W., "Infrared spectroscopic imaging for histopathologic recognition," Nat Biotechnol. 23, 469-474 (2005).

[8] McIntosh, L. M., Jackson, M., Mantsch, H. H., Stranc, M. F., Pilavdzic, D. and Crowson, A. N., "Infrared spectra of basal cell carcinomas are distinct from non-tumor-bearing skin components," J. Invest. Dermatol. 112, 951-956 (1999).

[9] Mohlenhoff, B., Romeo, M., Diem, M. and Wood, B. R., "Mie-type scattering and non-Beer-Lambert absorption behavior of human cells in infrared microspectroscopy," Biophys. J. 88, 3635-3640 (2005).

[10] Shaw, R. A., Guijon, F. B., Paraskevas, M., Ying, S. L. and Mantsch, H. H., "Infrared spectroscopy of exfoliated cervical cell specimens – proceed with caution," Anal. Quant. Cytol. 21**,** 292-302 (1999).

[11] E.g. the effect of cell turnover is characterized by Diem et al. (e.g. Boydston-White, S., Gopen, T., Houser, S., Bargonetti, J. and Diem, M., "Infrared spectroscopy of human tissue. V. Infrared spectroscopic studies of myeloid leukemia (ML-1) cells at different phases of the cell cycle," Biospectroscopy 5, 219-227 (1999)) in a number of articles and demonstrated quantitatively in a recent study that has implications for disease diagnoses Mourant, J. R., Yamada, Y. R., Carpenter, S., Dominique, L. R. and Freyer, J. P., "FTIR spectroscopy demonstrates biochemical differences in mammalian cell cultures at different growth stages," Biophys. J. 85, 1938–1947 (2003).

[12] Andrus, P. G., "Cancer monitoring by FTIR spectroscopy," Tech. Cancer Treat. Res. 5, 157-167 (2006).

[13] Bhargava, R., "Towards a practical Fourier transform infrared chemical imaging protocol for cancer pathology," Anal. Bioanal. Chem. 389, 1155-1169 (2007).

[14] Levin, I. W. and Bhargava, R., "Fourier transform infrared vibrational spectroscopic imaging: integration of microscopy and molecular recognition," Annu. Rev. Phys. Chem. 56, 429-474 (2005).

[15] Huang, D., Swanson, E. A., Lin, C. P., Schuman, J. S., Stinson, W. G., Chang, W., Hee, M. R., Flotte, T., Gregory, K., Puliafito, C. A. and Fujimoto, J. G., "Optical coherence tomography," Science 254,1178-1181 (1991).

[16] Fercher, A. F., Drexler, W., Hitzenberger, C. K. and Lasser, T., "Optical coherence tomography – principles and applications," Rep. Prog. Phys. 66, 239-303 (2003).

[17] Schmitt, J. M., "Optical coherence tomography (OCT): a review," IEEE J. Sel. Top. Quant. Elec. 5, 1205-1215 (1999).

[18] Schmitt, J. M., Knuttel, A., Yadlowsky, M. and Eckhaus, A. A., "Optical coherence tomography of a dense tissue: statistics of attenuation and backscattering," Phys. Med. Biol. 39, 1705-1720 (1994).

[19] Schmitt, J. M., Yadlowsky, M. J. and Bonner, R. F., "Subsurface imaging of living skin with optical coherence microscopy," Dermatology 191, 93-98 (1995).

[20] Sergeev, A. M., Gelikonov, V. M., Gelikonov, G. V., Feldchtein, F. I., Kuranov, R. V., Gladkova, N. D., Shakhova, N. M., Snopova, L. B., Shakov, A. V., Kuznetzova, I. A., Denisenko, A. N., Pochinko, V. V., Chumakov, Y. P. and Streltzova, O. S., "*In vivo* endoscopic OCT imaging of precancer and cancer states of human mucosa," Opt. Express 1, 432-440 (1997).
[21] Tearney, G. J., Brezinski, M. E., Boppart, S. A., Bouma, B. E., Weissman, N., Southern, J. F., Swanson, E. A. and Fujimoto, J. G., "Catheter-based optical imaging of a human coronary artery," Circulation 94, 3013 (1996).
[22] Tearney, G. J., Brezinski, M. E., Southern, J. F., Bouma, B. E., Boppart, S. A. and Fujimoto, J. G., "Optical biopsy in human gastrointestinal tissue using optical coherence tomography," Amer. J. Gastroenterol. 92, 1800-1804 (1997).
[23] Tearney, G. J., Brezinski, M. E., Southern, J. F., Bouma, B. E., Boppart, S. A. and Fujimoto, J. G., "Optical biopsy in human urologic tissue using optical coherence tomography," J. Urol. 157, 1915-1919 (1997).
[24] Bouma, B. E., Tearney, G. J., Boppart, S. A., Hee, M. R., Brezinski, M. E. and Fujimoto, J. G., "High resolution optical coherence tomographic imaging using a modelocked Ti:Al203 laser," Opt. Lett. 20, 1486-1488 (1995).
[25] Drexler, W., Morgner, U., Kartner, F. X., Pitris, C., Boppart, S. A., Li, X., Ippen, E. P. and Fujimoto, J. G., "In vivo ultrahigh resolution optical coherence tomography," Opt. Lett. 24, 1221-1223 (1999).
[26] Tearney, G. J., Bouma, B. E., Boppart, S. A., Golubovic, B., Swanson, E. A. and Fujimoto, J. G., "Rapid acquisition of in vivo biological images using optical coherence tomography," Opt. Lett. 21, 1408-1410 (1996).
[27] Tearney, G. J., Boppart, S. A., Bouma, B. E., Brezinski, M. E., Weissman, N. J., Southern, J. F. and Fujimoto, J. G., "Scanning single-mode fiber optic catheter-endoscope for optical coherence tomography," Opt. Lett. 21, 1-3 (1996).
[28] Boppart, S. A., Bouma, B. E., Pitris, C., Tearney, G. J. and Fujimoto, J. G., "Forward-imaging instruments for optical coherence tomography," Opt. Lett. 22, 1618-1620 (1997).
[29] Tearney, G. J., Brezinski, M. E., Bouma, B. E., Boppart, S. A., Pitris, C., Southern, J. F. and Fujimoto, J. G., "In vivo endoscopic optical biopsy with optical coherence tomography," Science 276, 2037-2039 (1997).
[30] Marks, D. L. and Boppart, S. A., "Nonlinear interferometric vibrational imaging," Phys. Rev. Lett. 92, 123905-1-4 (2004).
[31] Vinegoni, C., Bredfeldt, J. S., Marks, D. L. and Boppart, S. A., "Nonlinear optical contrast enhancement for optical coherence tomography," Opt. Express 12, 331-341 (2004).
[32] Applegate, B. E., Yang, C. and Izatt, J. A., "Theoretical comparison of the sensitivity of molecular contrast optical coherence tomography techniques," Opt. Express 13, 8146-8163 (2005).
[33] Ralston, T. S., Marks, D. L., Carney, P. S. and Boppart, S. A., "Interferometric synthetic aperture microscopy," Nat. Phys. 3, 129-134 (2007).
[34] Bhargava, R., Fernandez, D. C., Hewitt, S. M. and Levin, I. W., "High throughput assessment of cells and tissues: Bayesian classification of spectral metrics from infrared vibrational spectroscopic imaging data," Biochim Biophys Acta. 1758, 830-845 (2006).
[35] Choma, M. A., Sarunic, M. V., Yang, C. and Izatt, J., "Sensitivity advantage of swept source and Fourier domain optical coherence tomography," Opt. Express 11, 2183-2189 (2003).
[36] Leitgeb, R., Hitzenberger, C. K. and Fercher, A. F., "Performance of Fourier domain vs. time domain optical coherence tomography," Opt. Express 11, 889-894 (2003).
[37] Davis, B. J., Schlachter, S. C., Marks, D. L., Ralston, T. S., Boppart, S. A. and Carney, P. S., "Nonparaxial vector-field modeling of optical coherence tomography and interferometric synthetic aperture microscopy," J. Opt. Soc. Am. A 24, 2527-2542 (2007).
[38] Saleh, B. E. A. and Teich, M. C., [Fundamentals of Photonics], Wiley Series in Pure and Applied Optics, (1991).
[39] Davis, B. J., Marks, D. L., Ralston, T. S., Carney, P. S. and Boppart, S. A., "Interferometric synthetic aperture microscopy: computed imaging for scanned coherent microscopy," Sensors 8, 3903-3931 (2008).